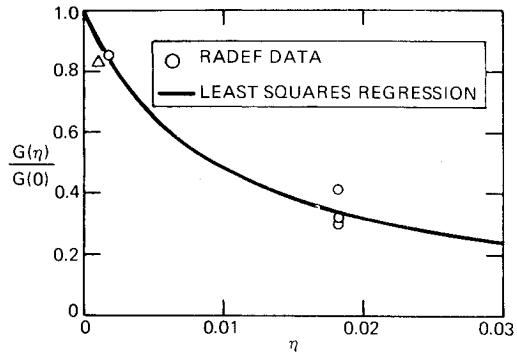

Fig. 2 Debris shielding at 5600 fps and at normal impact.

Because the quantities r' and C_D, the characteristic debris particle radius and drag coefficient, respectively, are not known accurately, it is convenient to define a new parameter η in which they do not appear

$$\eta = (w/\rho_l)(\rho_s R/\rho r)^{1/2} \tag{14}$$

$$= \eta'[(C_D/2)r/r']^{1/2} \tag{15}$$

In Eq. (6) we can now combine the quantity $(rC_D/2r')^{1/2}$ with the unknown mass loss ratio for the incoming drop G' to yield an unknown dimensionless coefficient B. This results in

$$G = G_o/(1+B\eta) \tag{16}$$

where the second term in the numerator has been neglected as discussed previously. In Eq. (16), G_o and B are considered to be empirical constants which can be determined by testing. These constants are clearly functions of test speed and impact angle and may depend on the test material.

It is worthwhile to note that the debris shielding analysis does not account for the shielding of the body by the aerodynamic shock layer itself. It has been shown[2] that for models of the size generally used in ballistic range tests, the shock layer does not provide shielding against dust particles of order 100 μ in diameter and larger or against precipitation-size water drops, which are of order 1 mm in diameter. We do not know, however, what effect the model shock layer might have on small ice particles, which may occur in rod, platelet, or branched dendritic forms. These particles have high drag and moment coefficients and therefore experience very high linear and angular accelerations. Moreover, these ice particles are relatively fragile (particularly the dendrites) and may be easily shattered, unlike small dust particles or larger raindrops. Thus, while it is reasonable to neglect the shielding effect of the model shock layer upon precipitating raindrops and dust particles, the effect upon ice crystals remains unknown and could possibly be significant. If such shielding occurs, the freestream air density will influence the measured mass loss ratio in a direction opposite to that indicated by Eqs. (14) and (16); that is, a higher air density will provide more aerodynamic shielding and thereby tend to reduce the measured value of G, while at the same time sweeping the debris away more quickly and thereby tending to increase that value.

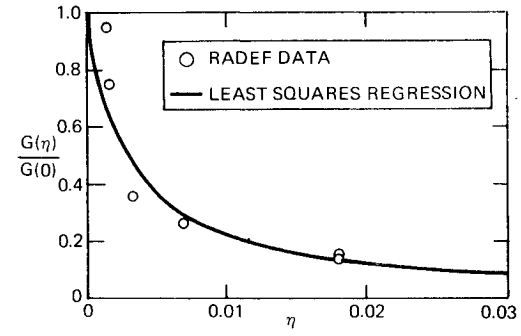

Fig. 3 Debris shielding at 14,000 fps and at normal impact.

A series of tests were conducted in the RADEF to measure debris shielding effects directly by varying the encountered water concentration from 10 to 140 g/m^3 while keeping all other test variables constant. The test model was a $\frac{1}{2}$-in.-diam flat-faced cylinder of a reinforced phenolic. The rain field consisted of 1-mm-diam water drops at 1 atm ambient pressure. The experimental mass loss data were all obtained in tests in which the sample had reached its asymptotic, multiple impact damage limit. The experiments were conducted at two speeds, 5600 and 14,000 fps. The test results, normalized by the empirically determined values of G_o, are shown in Figs. 2 and 3 plotted vs the dimensionless shielding parameter η. The lines in Figs. 2 and 3 represent least squares regressions of the form given in Eq. (16) and provide a satisfactory correlation of the data. The implication of these results is clear: debris shielding can significantly reduce the erosion experienced by a high-speed body, and relatively tenuous particle fields must be employed to obtain realistic erosion data.

References

[1] Reinecke, W., "Rain Erosion at High Speeds," *Proceedings of the Fourth International Congress on Rain Erosion*, Meersburg, Germany, May 1974.

[2] Waldman, G. and Reinecke, W., "Particle Trajectories, Heating, and Breakup in Hypersonic Shock Layers," *AIAA Journal*, Vol. 9, No. 6, June 1971, pp. 1040–1048.

Axisymmetric Buckling of Elastic-Plastic Annular Plates

A. NEEDLEMAN*
MIT, Cambridge, Mass.

I. Introduction

We consider an elastic-plastic annular plate subject to radial in-plane loading at its outer edge. The inner edge of the plate remains traction free and the outer edge the plate is taken to be either simply supported or clamped.

Depending on the thickness of the plate, bifurcation can occur while the plate is in a fully elastic, in a partly plastic, or in a fully plastic state. Attention is focused on cases where bifurcation occurs while the plate is in a partly plastic state and consideration is restricted to axisymmetric bifurcations.

Previous analysis of the buckling of elastic-plastic annular plates have either been of a very approximate character[1] or have employed a stability criterion that was, essentially, a generalization to plates of the reduced modulus theory for columns.[2,3] In this Note, the bifurcation analysis is formulated by means of tangent modulus theory.[4–6] Furthermore, an example is given of the postbuckling behavior and imperfection sensitivity of an annular plate, when bifurcation of the perfect plate takes place from a partly plastic state.

II. Problem Formulation and Numerical Analysis

The inner radius of the annular plate is specified by R_i and the outer radius by R_0. The loading is applied through a monotonically increasing radial compressive displacement U

Received March 14, 1974. This work was partially supported by NSF Grant GP 22796. During the course of this work the author visited the Department of Solid Mechanics, The Technical University of Denmark. Both the support and the hospitality of that department are gratefully acknowledged.

Index category: Structural Stability Analyses.

* Assistant Professor of Applied Mathematics.

at the plate's outer edge. Since the formulation employed here parellels that in Ref. 7, only certain aspects of the analysis will be discussed. Further details are given in Ref. 7.

The plate material is assumed to be strain hardening and characterized by J_2-flow theory with isotropic hardening. The uniaxial stress-strain behavior is modelled by a piecewise powerlaw with a continuous tangent modulus, i.e.,

$$\left(\frac{\varepsilon}{\varepsilon_y}\right) = \begin{cases} (\sigma/\sigma_y) & \sigma < \sigma_y \\ (1/n)(\sigma/\sigma_y)^n - (1/n) + 1 & \sigma \geq \sigma_y \end{cases} \tag{1}$$

where σ_y is the uniaxial yield stress, ε_y the uniaxial yield strain, and n the strain hardening exponent.

The incremental form of the von Kármán strain-displacement equations[8] are employed and incremental equilibrium is expressed in terms of a variational principle. This variational principle is then used as the basis for implementing a finite element solution. Both the in-plane and lateral displacement increments are expressed in terms of Hermitian cubic polynomials within each element. The loading history is calculated in the incremental fashion described in Ref. 7.

For a perfect plate, the bifurcation calculation proceeds as follows. An increment of the in-plane prebifurcation solution is calculated. The stiffness matrix for out of plane bending is then assembled. In this calculation, the plastic loading branch of the plane stress moduli is employed throughout the current plastic zone. This stiffness matrix is factored as in Ref. 9. If the determinant of this stiffness matrix is zero, the bifurcation mode is calculated and the computation terminates. On the other hand, if the determinant is positive, linear extrapolation of a quantity that governs the sign of the determinant (the smallest diagonal element of the factored stiffness matrix) is used to predict whether the determinant will be negative at the next increment. When the determinant is predicted to be negative at the next stage of the loading history, the increment size is reduced.

In order to assess the accuracy of this procedure, the bifurcation stress of a simply supported elastic-plastic circular plate ($R_i = 0$) was determined by the preceding procedure. The numerical value agreed with the analytical result[7] to four significant figures.

The average applied stress at the plate's outer edge is denoted by σ_{ave} and given by

$$\sigma_{ave} = -\frac{1}{t}\int_{-t/2}^{t/2} \sigma_r(R_0, z)\, dz \tag{2}$$

Here, t is the plate thickness and σ_r is the radial stress component. Note that σ_{ave} is defined to be positive for compressive loading.

For an elastic circular plate of radius R_0 and thickness t subject to radial compressive loading, the value of the bifurcation stress, is given by[8]

$$\sigma_0 = \frac{\beta_E{}^2 E}{12(1-\nu^2)}\left(\frac{t}{R_0}\right)^2 \tag{3}$$

where E is Young's modulus and ν is Poisson's ratio. The value of β_E depends on the boundary conditions. For a clamped plate $\beta_E = 3.832$, while for a simply supported plate with $\nu = \frac{1}{3}$, $\beta_E = 2.069$. Here, it is convienient to characterize the thickness to outer radius ratio, t/R_0, of an annular plate, by the following parameter

$$\rho = \sigma_0/\sigma_y \tag{4}$$

III. Results

Figures 1 and 2 display curves of the average stress at bifurcation σ_c, vs R_i/R_0, for $\nu = \frac{1}{3}$, $n = 12$; in Fig. 1, $\rho = 0.72$ while in Fig. 2, $\rho = 0.99$.

For both these values of the thickness parameter ρ, bifurcation of a circular plate ($R_i = 0$) occurs prior to initial yielding. However, for annular plates ($R_i \neq 0$) with $\rho = 0.72$ and $\rho = 0.99$, plastic yielding begins at the inner radius $r = R_i$, prior to bifurcation. The effect of plastic yielding becomes more significant as the ratio of inner radius to outer radius, R_i/R_0, increases.

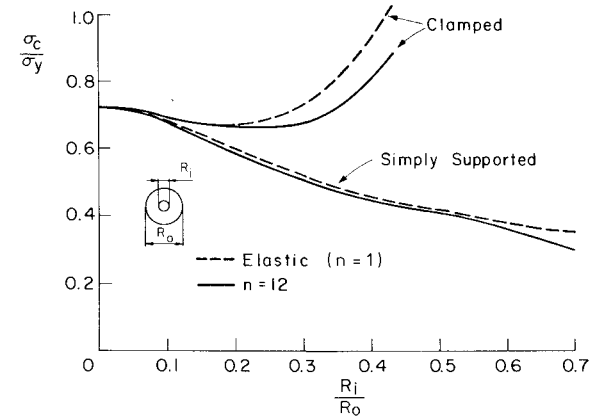

Fig. 1 Bifurcation stress vs hole radius for annular plate ($\nu = \frac{1}{3}$, $\rho = 0.72$).

Also displayed in Figs. 1 and 2 are the bifurcation results of elastic plates ($n = 1$). The elastic bifurcation stresses were obtained by the same numerical method as that employed in the elastic-plastic calculations and agree with the results given in (Ref. 8, p. 392).

For a simply supported plate, the critical stress σ_c is a monotonically decreasing function of R_i/R_0. However, for a clamped plate, the buckling load initially decreases as a function of R_i/R_0, reaches a minimum at about $R_i/R_0 = 0.2$ and then is a rapidly increasing function of R_i/R_0. Undoubtedly, for R_i/R_0 greater than about 0.2 there is some other buckling mode, either a nonaxisymmetric bending mode or an in-plane mode, that has a critical stress lower than that for axisymmetric bending. Here, no attempt is made to investigate these possibilities.

In Fig. 1, for the simply supported boundary condition, it can be seen that the buckling loads predicted by an elastic-plastic analysis are nearly the same as those obtained from a purely elastic analysis when $R_i/R_0 < 0.5$. In this range bifurcation occurs shortly after initial yielding. However, for $R_i/R_0 = 0.7$, the bifurcation stress of an elastic-plastic plate is 14% lower than that for an elastic plate. In this case, at bifurcation the elastic-plastic boundary is at 0.8 R_0.

In Fig. 2, where $\rho = 0.99$, there is a significant discrepancy between the elastic plastic and the elastic results even for $R_i/R_0 = 0.1$. At bifurcation, for a simply supported plate, the elastic-plastic boundary is at 0.19 R_0 for $R_i/R_0 = 0.1$ and at 0.86 R_0 for $R_i/R_0 = 0.7$.

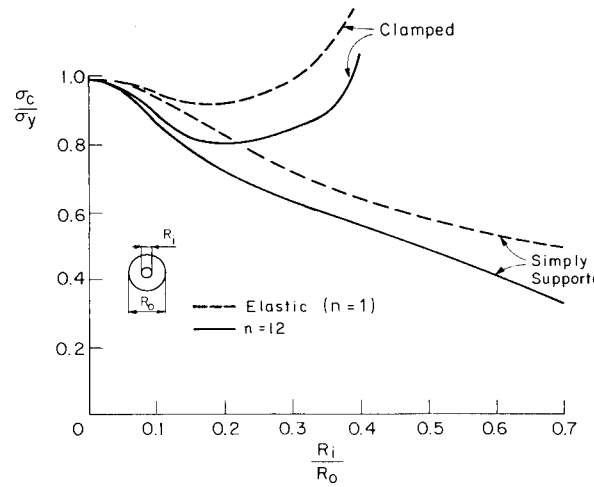

Fig. 2 Bifurcation stress vs hole radius for annular plate ($\nu = \frac{1}{3}$, $\rho = 0.99$).

Finally, we consider an example of the postbuckling behavior and imperfection sensitivity of an annular plate. In Fig. 3, average stress-end shortening and average stress-buckling deflection curves are shown for a simply supported annular plate with $\nu = \frac{1}{3}$, $n = 12$, $R_i/R_0 = 0.4$, $\rho = 1.28$, and $\sigma_c/\sigma_y = 0.61$. The bifurcation stress for a similar plate with purely elastic material response ($n = 1$) is $\sigma_c/\sigma_y = 0.82$.

The imperfection is taken to be proportional to the buckling mode obtained from the bifurcation analysis. The buckling mode $\hat{w}(r)$, is normalized so that $\hat{w}(R_i) = 1$ and the imperfection amplitude is denoted by $\bar{\xi}$. The buckling deflection is measured by ξ where

$$\xi = w(R_i) - \bar{\xi} \tag{5}$$

here $w(R_i)$ is the lateral deflection at the plate's inner edge. Furthermore, the results given here for a "perfect" plate are actually the results of a calculation using a small imperfection, $\bar{\xi} = 10^{-4}t$.

In Fig. 3a, the applied edge displacement U is normalized by U_y, that value of U at which initial yielding occurs in the perfect plate. Also shown is the average stress-applied displacement curve for the prebuckling solution. Note that for a perfect plate, the curve continues to rise after bifurcation and differs little from the corresponding curve of the prebuckling solution until the maximum load has been reached.

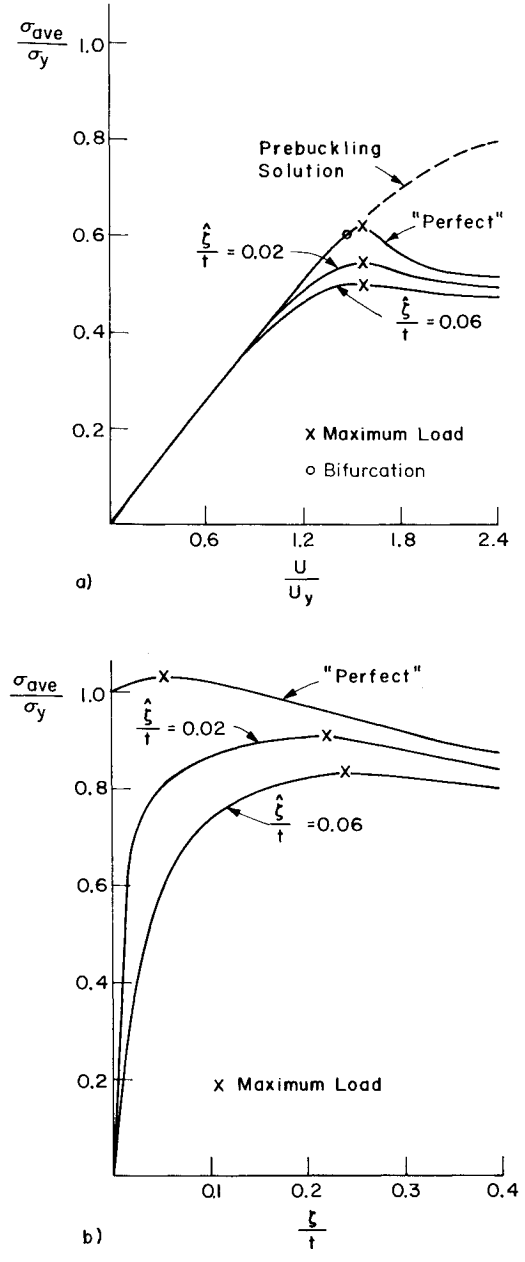

Fig. 3 Postbuckling curves for a simply supported annular plate ($\nu = \frac{1}{3}$, $n = 12$, $R_i/R_0 = 0.4$, $\rho = 1.28$, $\sigma_c/\sigma_y = 0.61$). a) Average stress-applied displacement. b) Average stress-buckling deflection.

At bifurcation the elastic-plastic boundary of the perfect plate has reached $r = 0.53\ R_0$, and unloading begins at $r = R_i = 0.4\ R_0$ and $z = t/2$. At the maximum load point, this side ($z = t/2$) of the plate has completely unloaded while on the opposite side of the plate the plastic zone extends to $r = 0.79\ R_0$. This side continues to load plastically until the entire side has yielded. During the latter stages of deformation shown in Fig. 3, a region near $r = R_i = 0.4$, $z = t/2$ has yielded in tension.

This example was chosen because bifurcation occurs at the "knee" of the average stress-applied displacement curve of the prebifurcation solution. The postbuckling behavior of the perfect plate is qualitatively similar to that of a circular plate for which the bifurcation stress is near σ_y.[7] The imperfection sensitivity of the annular plate is not as great as that of the circular plate, but is still significant. For an imperfection amplitude $\bar{\xi} = 0.06\ t$ the maximum load is 82% of the bifurcation load.

Thus, annular plates can be imperfection sensitive when bifurcation of the perfect plate occurs from a partly plastic state.

References

[1] Gajewski, A. and Zyczkowski, M., "Elastic-Plastic Buckling of Some Circular and Annular Plates of Variable Thickness," *Polska Akademia Nauk, Se'riedes Sciences Techniques*, Vol. 14, 1966, pp. 313–320.

[2] Foral, R. F. and Gerstle, K. H., "The Stability of an Annular Plate of Strain Hardening Material," *Proceedings of the Tenth Midwestern Mechanics Conference, Developments in Mechanics*, Vol. 4, 1968, pp. 347–365.

[3] Foral, R. F. and Hodge, P. G., Jr., "A Consistent Theory for the Elastic-Plastic Stability of an Annular Plate Under Inner Tension," Rept. Hl-2, Dept. of Aerospace Engineering and Mechanics, Univ. of Minnesota, Minneapolis, Minn., Vol. 14, No. 5, May 1947.

[4] Shanley, F. R., "Inelastic Column Theory," *Journal of Aerospace Science*, Vol. 14, 1947, pp. 261–267.

[5] Hill, R., "Bifurcation and Uniqueness in Nonlinear Mechanics of Continua," *Problems of Continuum Mechanics*, Society for Industrial and Applied Mathematics, Philadelphia, Pa., 1961, pp. 155–164.

[6] Sewell, M. J., "A General Theory of Elastic and Inelastic Plate Failure—I," *Journal of Mechanics and Physics of Solids*, Vol. 11, 1963, pp. 377–393.

[7] Needleman, A., "Posbifurcation Behavior and Imperfection Sensitivity of Elastic-Plastic Circular Plates," *International Journal of Mechanical Science* (to be published).

[8] Timoshenko, S. P. and Gere, J. M., *Theory of Elastic Stability*, 2nd ed., McGraw-Hill, New York, 1961.

[9] Needleman, A., "A Numerical Study of Necking in Circular Cylindrical Bars," *Journal of the Mechanics and Physics of Solids*, Vol. 20, No. 2, May 1972, pp. 111–127.

Value of Mach Angle for a Given Prandtl-Meyer Angle

WILLIAM J. H. SMITHEY*
Naval Postgraduate School, Monterey, Calif.

THIS Note presents a numerical method for determining the Mach angle μ for a given value of the Prandtl-Meyer angle ν.

Received March 11, 1974. This work was supported by the Naval Ordnance Station, Indian Head, Md.

Index category: Supersonic and Hypersonic Flow.

* Commander, U.S. Navy; also Graduate Student, Department of Aeronautics.